Journal of Colloid and Interface Science **245,** 75–80 (2002)
doi:10.1006/jcis.2001.8005, available online at http://www.idealibrary.com on IDEAL®

Confocal Microscopy of a Dense Particle System

E. H. C. Bromley and I. Hopkinson[1]

Cavendish Laboratory, University of Cambridge, Madingley Road, Cambridge CB3 0HE, United Kingdom

Received May 21, 2001; accepted October 1, 2001

We report experiments utilizing confocal microscopy to determine the position of cornflour starch granules in a paste, as a function of distance from a wall. The granules have an average diameter of 15 μm. If a solvent is chosen such as to approximately match the refractive index of the granules then images of them can be obtained to a depth of 120 μm, which is the limit imposed by the working distance of the x40 oil immersion lens used in the experiment. An algorithm is presented which successfully identifies the particle centers in 3D. In addition to experiments on static systems we show how measurements of particle number density and velocity can be obtained from images of a system in pipe flow. We find that particles are depleted from the wall over a range of around 100 μm.

Key Words: **confocal microscopy; suspension flow; wall effects.**

INTRODUCTION

The behavior of particle-bearing systems is of very widespread industrial interest; such systems exhibit non-Newtonian and complex flow behavior (1, 2). There is vigorous theoretical and simulation activity in understanding the flow behavior of, in particular, granular media and colloidal suspensions. Experimentally the rheology of such systems has long been studied. Light scattering has been used to probe the structure of suspensions, particularly colloidal suspensions, under flow (3). In terms of granular materials the geometric arrangement of particles and their contacts is important (4).

Here we present images and analysis of a cornflour paste, both stationary and under flow acquired using confocal microscopy. The advantages of this technique are high spatial resolution and relatively short acquisition time when compared to other direct imaging techniques. The disadvantages are the requirement for a close refractive index match between particle and suspending medium and a restricted imaging volume. In contrast to scattering methods, microscopy does not volume average so that local behavior, such as the high mobility of a small fraction of the sample as it approaches a glass transition, can be identified (5, 6).

Confocal microscopy was originally proposed by Minsky (7); however, it was not until the 1980s that technology became available which enabled a realization of a confocal microscopy which was suitable for routine use. Since this time several generations of microscopes have been produced. Such microscopes have been used very widely in biology (8), but it has only been more recently that the potential for application to problems in physics and chemistry has been realized and acted upon (9, 10).

The key feature of the confocal microscopy is that a pinhole in the detection optics excludes light from all but the focal plane. This is in contrast to conventional (or wide-field) microscopy where light from the focal plane is mixed with out of focus light from above and below the focal plane. This feature makes it possible to acquire a three-dimensional picture of a sample at high resolution. In general image acquisition requires that a laser be scanned over the sample in the x-y plane and the sample stage translated in the z-direction to acquire a 3D volume of data. Acquisition times are of the order 1 s per x-y plane and around 1 min for a stack of 50 images. Images can be acquired at video rates (50 Hz), by using a Nipkow disk instrument, which replaces a single stationary pinhole with multiple pinholes mounted on a spinning disk. However such instruments have the disadvantages of poor light efficiency and fixed pinhole size (11).

There are a number of alternatives to confocal microscopy in determining the microscopic structure and flow behavior of particle suspensions. MRI can directly image flow fields in complex geometries (12). Acquisition time is comparable to the confocal experiments we present here. Resolution is limited, but the imaging volume is only restricted by the size of the magnet bore. X-ray tomography also offers a method to image particle beds (13); a particular advantage is that granular materials in air can be imaged. Resolution and imaged volume are both good but data acquisition time is slow and data analysis is complex.

Cornflour is composed entirely of starch granules 15–25 μm in diameter. They were chosen for this study for several reasons: cornflour/water is a well-known non-Newtonian system (14), and particles are small, relatively monodisperse, and cheap. Starch granules are composed of a mixtures of long-chain polysaccharides with varying degrees of branching along with a range of minor components. Structurally the polysaccharides are organized in alternating crystalline and amorphous growth rings (15). This is of importance to this work, since it means that the interior of the granule is heterogeneous in refractive index.

We anticipate two problems in attempting to image starch granule pastes. First, if the solvent in which the granules are

[1] To whom correspondence should be addressed. Fax: +44 (0)1223 337 000. E-mail: Ian.Hopkinson@phy.cam.ac.uk.

0021-9797/02 $35.00

suspended is not refractive-index-matched to the granules then there will be strong reflections from the interfaces. If we wish to image a significant distance into the paste then this will require light to traverse many such interfaces and so minimizing the refractive index step will be critical. Secondly, the interior of the granule may scatter light through its heterogeneous structure.

MATERIALS AND METHODS

Confocal images were acquired using a Zeiss LSM510 upright confocal microscope. 0.1 wt% Nile red was used to fluorescently label the continuous phase. The dye was excited at 543 nm, and light from the sample was filtered by a 560 nm long pass filter before detection using a PMT. Images were acquired with an x40 oil immersion lens with 120 μm working distance and NA = 1.3. Acquisition times were typically 1 s per x-y image and 1 min for 3D stacks.

Commercial grade cornflour was used throughout with no further processing. Preliminary experiments were carried out to identify the best suspending solvent, and suitability of a solvent was measured by the ability to image through several layers of starch granules. Candidate solvents were selected on the basis that the best would refractive-index-match the starch granule. We estimated the refractive index of starch granules to be around 1.54, based on the refractive index of sucrose (which is chemically very similar to starch). Benzyl alcohol (RI = 1.5404) was found to be most suitable. A mismatch between the refractive index of the objective immersion oil and the sample leads to spherical aberration (16, 17). The Zeiss immersion oil used in this work has a refractive index of 1.518. Trial images taken using ethyl-4-ethoxybenzoate as the suspending medium, which exactly refractive index matches the immersion oil, showed marginally better depth penetration than that observed in benzyl alcohol. However ethyl-4-ethoxybenzoate was less readily available and given it only provided a slight improvement in image quality, benzyl alcohol was used for the remainder of the work.

Samples used for static imaging were prepared by mixing the desired weights of solvent and starch granules thoroughly and placing the resulting paste in "deep well" cells. These comprised a ring or plate glued onto a glass slide. The well depth was 3 mm and the diameter 10 mm. A coverslip was then placed on top of the paste, where it was held by capillary forces. Where an oil immersion lens was used small spots of clear nail varnish were used to hold down the coverslip.

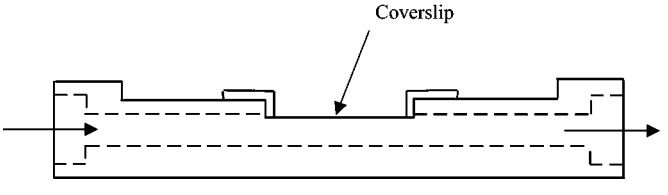

FIG. 1. Schematic diagram of the flow cell in cross section. Broken lines indicate internal bore.

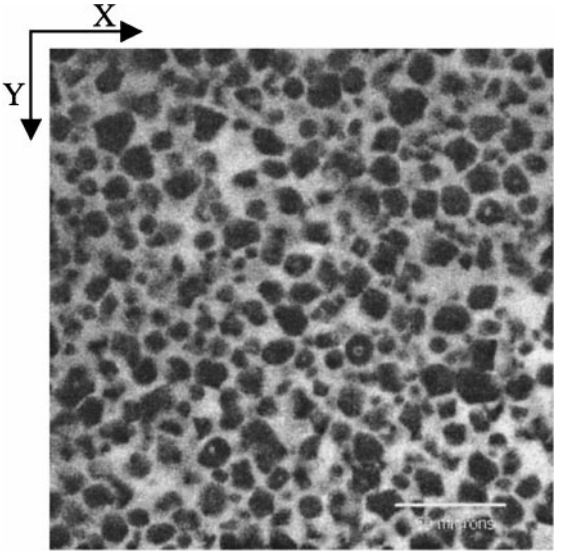

FIG. 2. x-y image of a starch-benzyl alcohol paste using x40 objective, 54 μm below upper surface (scale bar 50 μm).

A simple "pipe flow" cell was constructed, this is shown schematically in Fig. 1. The cell comprises a brass monolith approximately 30 × 10 × 100 mm with a 7-mm-diameter circular cross-section hole drilled down the center, along the longest dimension. A 40-mm-length insert was removed from the top of the block, revealing a rectangular face of the hole. A large glass coverslip was glued over the exposed pipe. Cornflour paste was pumped through the drilled hole using a syringe pump. Although a nominal flow rate could be applied the actual flow rate fluctuated considerably. Sequences of six images were acquired once flow had been established, this process was repeated for a number of different distances from the coverslip.

Figure 2 shows an x-y image of a static sample, acquired using the x40 objective. Particles appear dark and the suspending solvent appears bright due to the presence of the fluorescent dye. Figure 3 shows a vertical section through a paste which extends

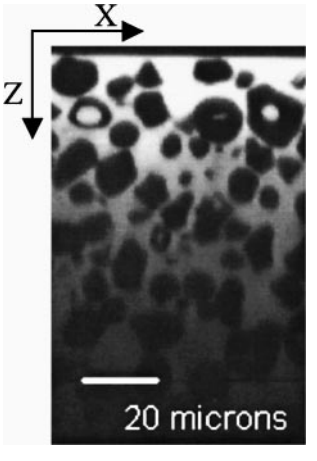

FIG. 3. Vertical section (x-z) through starch-ethyl-4-ethoxybenzoate paste (scale bar 20 μm).

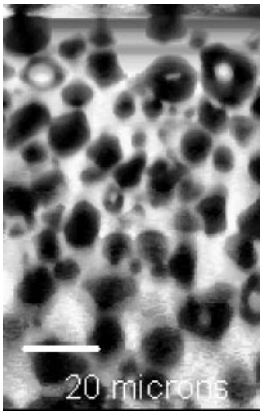

FIG. 4. Vertical section (x-z) through starch-ethyl-4-ethoxybenzoate paste with each horizontal line contrast enhanced (scale bar 20 μm).

to the working distance limit of the objective used, 120 μm. Although there is substantial darkening of the image with depth, some contrast between particle and suspending solvent does remain. This is illustrated in Fig. 4. Here each "horizontal" line in the image is independently contrast-enhanced and structure is clearly revealed to the working distance limit. Image quality is reduced toward the bottom of the image. Contrast was also observed in reflected light images, and the cores of some starch granules appeared as speckled patches of light. This effect arises from the heterogeneity in refractive index of the starch granule. Reflected light contrast indicates that light is being scattered by the granules and as such it is probably responsible for the degradation of image quality and brightness at increased depth. Although this is an interesting effect we do not utilize it further in investigating the structure of our suspensions because the contrast does not arise in all particles and does not delineate the whole starch granule.

RESULTS AND DISCUSSION

It was possible to image cornflour in benzyl alcohol pastes to a depth of around 100 μm. Typically an imaged volume contained around 800 granules, as identified by the 3D particle-finding algorithm described below. The overall average phase volume of the starch granules was around 0.45, although this covers a variation from around 0.35 at the upper surface to 0.55 at depth. These volume fraction figures are somewhat tentative since it depends on the thresholding of the images.

Ideally we wish to extract particle centers and contact points from volume images such as those illustrated in Figs. 2 and 3. The first step in this process is to identify and separate the individual particles in the paste. Simple intensity threshold algorithms do not work on this system. This is because of the close packing of the particles and the variation in intensity of individual particles which leads to either underthresholding with individual particles much reduced in size and many particles missed completely or overthresholding with several particles being lumped together as one. This type of problem is often overcome using a "watershed" algorithm (18); however, this results in the identification of too many particles—with single particles being split. We use an algorithm, described below, which has some similarity to the "watershed." The algorithm was implemented in both 2D and 3D:

(1) Images are thresholded at the mean image intensity for each slice, with a cut off "minimum" threshold.

(2) A Gaussian blur is applied to the image, the width of which depends on the sample and spans several particle diameters. For the 3D algorithm the convolution is applied in 3D.

(3) Particle centers are then identified with local maxima in the blurred image, a minimum separation radius is defined which prevents the identification of multiple adjacent centers which can arise from broken starch granules. In the 3D algorithm this locates the particle centres with an (x, y, z) coordinate.

Figure 5 shows an example of the centers identified by the 2D algorithm in a typical image. The white points appear to locate the centers of particles with a fair degree of accuracy. In some cases objects which would be identified as two particles due to their irregular perimeter are identified as a single particle, conversely some single particles are marked with two prospective centers by the algorithm. In this 2D image of order 4% of particles are not marked, and around 1% are double marked. The effectiveness of the algorithm in 3D is rather more difficult to illustrate but appears to be at least as good as the algorithm in 2D.

The particle center data can be used to determine the radial distribution function; this is shown in Fig. 6. We see that there is an exclusion zone to 7 μm which corresponds to a minimum granule size and that there is a peak in the distribution function at 18 μm which corresponds to the "mean" first coordination shell. These data are consistent with the bond length distributions we

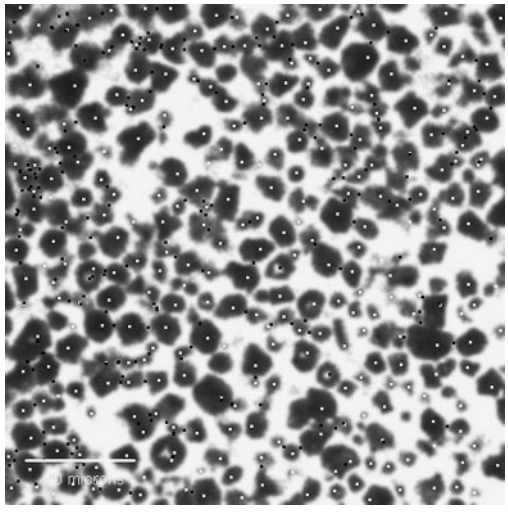

FIG. 5. x-y image of starch-benzyl alcohol paste with particle centers (white spots) and interparticle contacts (black spots) identified using the algorithm described in text (scale bar 50 μm).

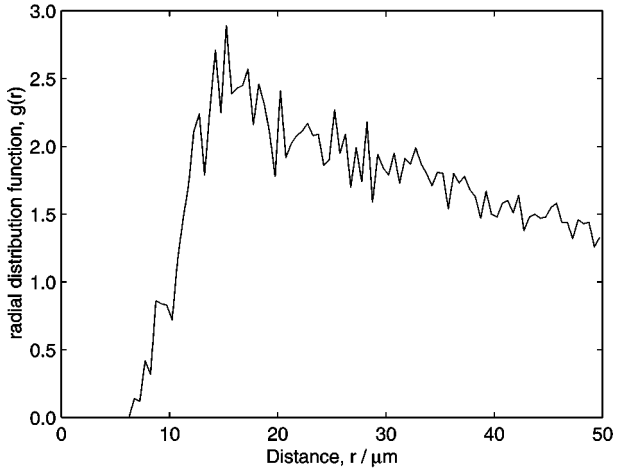

FIG. 6. Radial distribution function for a starch-benzyl alcohol paste.

obtain below and with direct observations of particle size. Beyond the first coordination shell there is no structure to the radial distribution function. In a system of monodisperse spheres this could be interpreted as indicating that the system was "gaseous." However in a system of polydisperse irregular particles it is less clear that this would be the case.

In addition to identifying particle centers we would like to identify the network of contacts between particles. This is a difficult task for irregular particles. We can make an approximation by selecting the nearest neighbors of a particle up to some distance. A line between the centers of the two particles is examined. If the intensity along the line rises above a user-defined intensity then the particles are deemed not to be in contact since the rise in intensity corresponds to the presence of fluorescent solvent lying between them. If the intensity does not reach the threshold value then the contact is marked as the point of maximum intensity along the line of centers. Figure 5 includes the contacts identified in a 2D system in this way. Around 10% of marked contacts are spurious. They serve to identify prospective

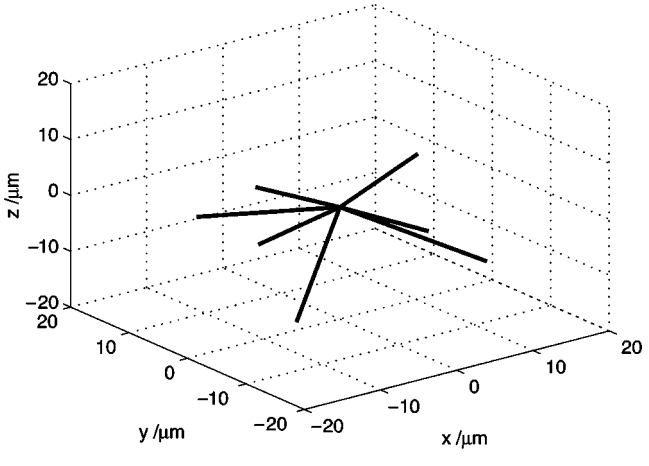

FIG. 7. First coordination shell for a selected starch granule.

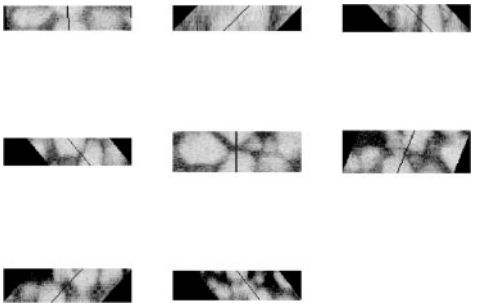

FIG. 8. Image intensity profiles along the bonds to the first coordination shell identified in Fig. 7.

contacting particles although not necessarily the contact point. The errors in identifying particle centers described above lead to a number of contact misidentifications.

We now turn to the identification of contacts in 3D. Fig. 7 shows the prospective center to center lines (or "bonds") to the first shell of contacting particles for a single particle. Figure 8 shows images aligned along the bonds illustrated in Fig. 7. These bonds were identified using a cutoff distance of 20 μm, chosen with reference to the radial distribution function which indicates a first coordination shell at 18 μm. Cutoff distances larger than this tended to give unphysically large numbers of contacts. In this instance a high threshold value was used to identify contacts. Figure 9 shows the effect that the threshold value has on the coordination number distribution. The broken line shows the distribution for a very high threshold (i.e., all neighbors identified as contacts). The solid line shows the distribution for a lower threshold level, which excludes many of the neighbors from being identified as contacts. Both curves show some sort of maximum at a coordination number of 6, consistent with the radial distribution function which suggests liquid-like behavior.

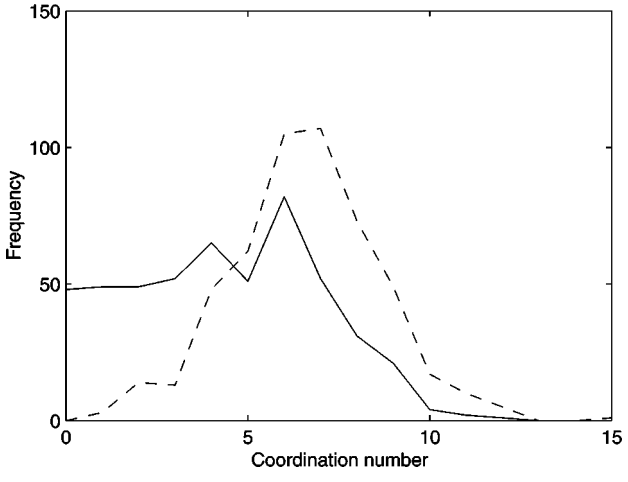

FIG. 9. Coordination number distribution (a) contacts identified by threshold (solid line), (b) all neighbors within 20 μm identified as contacts (broken line).

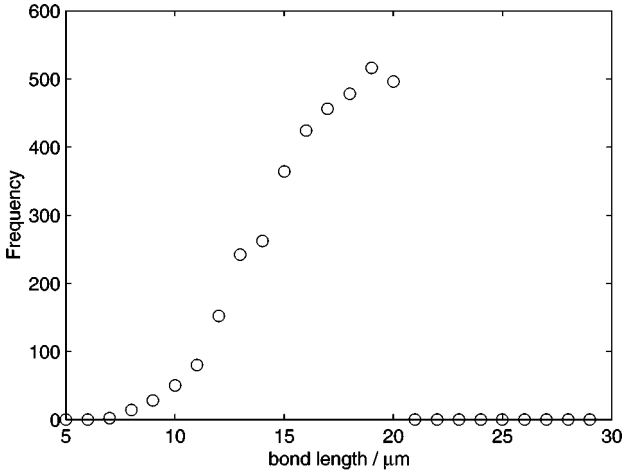

FIG. 10. Bond length distribution plot; 20-μm cutoff is imposed.

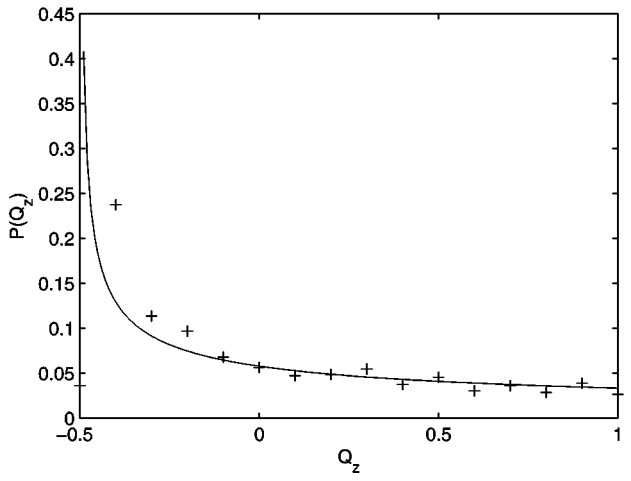

FIG. 11. Bond order parameter distribution relative to surface normal (+) and prediction for isotropic distribution (line).

The images in Fig. 8 (and analysis of similar images) suggest that in approximately 50% of cases contact is not seen on the center to center line, although it is possible that two irregular particles can touch away from this line. Some confusion is introduced by the presence of small particles, which bridge between identified particles.

The bond length distribution is shown in Fig. 10. It has a maximum at 18 μm with the imposed cutoff apparent at 20 μm. The distribution is extended on the low size side. The bond length distribution should be related to the particle size distribution, and qualitatively this is the case. The extended tail of smaller sizes is consistent with the presence of smaller starch granules and a few granule fragments.

In summary our algorithm for identifying contacts is not particularly successful. The bonds generated are effectively the nearest neighbor coordination shell rather than the nearest *contacting* neighbor coordination shell. Confounding factors are the irregularity of the particles which means that the contacts do not necessarily lie on the center to center line upon which the contact check is made, variations in the maximum intensity between particles make thresholding difficult, and finally identifying contacts "by eye" is not easy making it hard to confirm the efficiency of any particular automatic algorithm.

Despite these provisos we can still calculate the nematic order parameter distribution for these bonds to the nearest neighbors, although we should be clear that this is not the distribution function for contacts. The nematic order parameter is defined as

$$Q_n = \frac{1}{2}[3\cos^2(\phi_n) - 1], \qquad [1]$$

where ϕ_n is the angle made with the reference vector. For an isotropic distribution of bond directions the expected distribution function is given by

$$P(Q_n) = 1/\sqrt{6Q_n + 3}. \qquad [2]$$

Figure 11 shows the measured order parameter distribution function relative to the normal (z) direction, along with a theoretical prediction from [2]. We can see that the match is very good, suggesting that the bonds to the first coordination shells in the system are oriented isotropically.

We were also able to acquire data from the cornflour system under flow. It was found that the starch granules sedimented in benzyl alcohol and the flow observed tended to be of a highly inhomogeneous nature, with regions of aggregated starch granules undergoing little or no flow and other regions of lower density undergoing rapid flow. We were able to observe some uniform flow near the upper face of the sample cell and it is on these data we perform further analysis.

The overall volume fraction for the data analyzed here is around 0.5. Figure 12 shows a comparison between the 2D

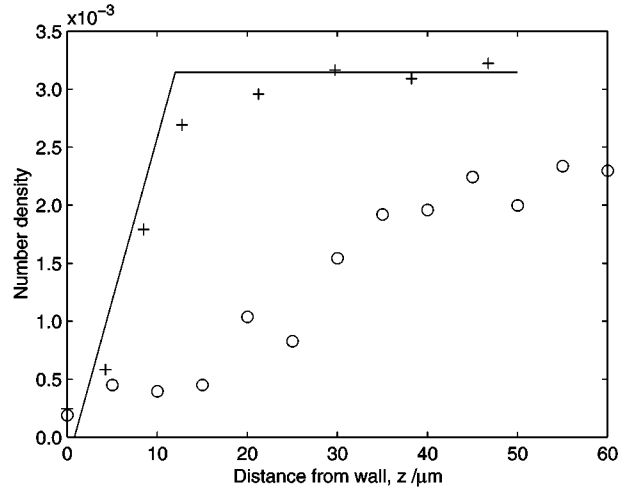

FIG. 12. 2D number density of particles from the upper surface of the sample, for a static paste (+) and for a paste in flow (○). Including a prediction for the static case from geometric exclusion (line).

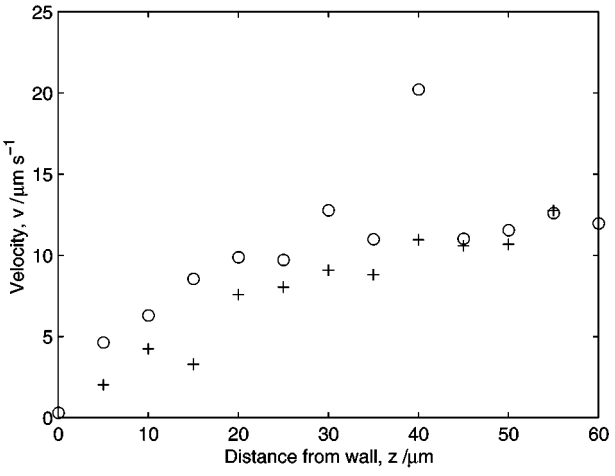

FIG. 13. Particle velocity profiles in the vicinity of the wall for two independent experiments on a 0.5 vol fraction starch-benzyl alcohol paste.

number density of granules close to a wall for a static sample and for a sample undergoing flow. The static sample shows a depletion of particle centers from the wall which can be modeled entirely by simple geometric exclusion. Under flow there is a clear depletion of particles from the wall extending over at least 60 μm, Linear extrapolation would suggest a depletion layer of around 100 μm. We can measure a velocity gradient in this region, and this was done by acquiring a sequence of 6 consecutive images in the plane of interest and then estimating the vector required to overlay the images. A refinement of this initial guess vector is then made using a computer program which maximizes the intensity correlation function, $G(t, t')$:

$$G(t, t') = \langle 1 - 2[I(x, y, t) - I(x + \Delta x, y + \Delta y, t')]^2 \rangle_{x,y}. \quad [3]$$

$I(x, y, t)$ is the intensity of a point (x, y) in the image at time t. $(\Delta x, \Delta y)$ is a prospective offset vector. From these displacement vectors and the known time between images the particle velocity can be calculated. The results of these velocity profile calculations are shown in Fig. 13. Two independent runs are shown and they agree remarkably well. Although there are fluctuations the shear gradient appears linear with displacement from the wall, over the small distance observed. The shear gradient is 0.2 s^{-1}. A useful dimensionless group in describing suspension flow is the Peclet number (3);

$$Pe = \frac{6\pi\dot{\gamma}\eta_0 a^3}{8k_B T}, \quad [4]$$

where a is the particle diameter, η_0 is the solvent viscosity, $\dot{\gamma}$ is the shear rate, T is the temperature, and k_B the Boltzmann factor. The measured shear rate corresponds to $Pe \gg 1$, confirming that the flow is shear-dominated and Brownian forces are unimportant—as would be expected for such large particles. The shear rate is below the rate at which shear thickening has been observed in starch suspensions of this volume fraction, but is of a similar order of magnitude (14).

SUMMARY

We have shown that confocal microscopy can be used to image significant numbers of irregular particles in a paste, although careful selection of the suspending fluid was required to avoid problems arising from a refractive index mismatch between particle and fluid. We have developed algorithms which can be used to successfully identify particle centers. A simple algorithm to find contact points between particles was not very successful. Images of the cornflour paste under flow were also acquired and flow profiles in the vicinity of the wall were determined. There is a depletion of particles from the wall during flow over a range of around 100 μm. However, the flow field was very heterogenous and it will require further work to make a more definite conclusion. The onset of sedimentation represents a clear challenge to the flow measurements; however, to overcome this problem it is necessary to both density match and refractive index match to maintain viewability.

The identification of interparticle contacts is a difficult problem and would probably be best addressed by a method in which the contact points were "physically" labeled. This could be done using fluorescent energy transfer in a dual-labeled particle system. Fluorescence of the acceptor excited at the donor frequency would only occur where differently labeled particles are in close contact.

REFERENCES

1. Barnes, H. A., *J. Non-Newtonian Fluid Mech.* **56,** 221 (1995).
2. Werff, J. C. v. d., and Kruif, C. G. d., *J. Rheol.* **33,** 421 (1989).
3. Clarke, S. M., Ottewill, R. H., and Rennie, A. R., *Adv. Colloid Interf. Sci.* **60,** 95 (1995).
4. Edwards, S. F., and Grinev, D. V., *Chaos* **9,** 551 (1999).
5. Weeks, E. R., Crocker, J. C., Levitt, A. C., Schofield, A. , and Weitz, D. A., *Science* **287,** 627 (2000).
6. Kegel, W. K., and Blaaderen, A. v., *Science* **287,** 290 (2000).
7. Minsky, M., *Scanning* **10,** 128 (1988).
8. "Handbook of Biological Confocal Microscopy" (J. B. Pawley, Ed.). Plenum, New York, 1995.
9. Ribbe, A. E., *Trends Polym. Sci.* **5,** 333 (1997).
10. Chestnut, M. H., *Curr. Opin. Colloid Interf. Sci.* **2,** 158 (1997).
11. "Confocal Microscopy" (T. Wilson, Ed.). Academic Press, London, 1990.
12. Callaghan, P. T., *Rep. Progr. Phy.* **62,** 599 (1999).
13. Seidler, G. T., Martinez, G., Seeley, L. H., Kim, K. H., Behne, E. A., *et al., Phys. Rev. E* **62,** 8175 (2000).
14. Frith, W. J., and Lips, A., *Adv. Colloid Interf. Sci.* **61,** 161 (1995).
15. Waigh, T. A., Hopkinson, I., Donald, A. M., Butler, M. F., Heidelbach, F., *et al., Macromolecules* **30,** 3813 (1997).
16. Visser, T. D., Groen, F. C. A., and Brakenhoff, G. J., *J. Microsc.* **163,** 189 (1991).
17. Hell, S., Reiner, G., Cremer, C., and Stelzer, E. H. K., *J. Microsc.* **169,** 391 (1993).
18. Russ, J. C., "The Image Processing Handbook." CRC Press, London, 1994.